

# Anisotropy of flow in stochastically generated porous media

Maciej Matyka, Zbigniew Koza, and Jarosław Golembiewski  
*Faculty of Physics and Astronomy, University of Wrocław, 50-204 Wrocław, Poland*

Marcin Kostur and Michał Januszewski  
*Institute of Physics, University of Silesia, 40-007 Katowice, Poland*  
 (Dated: August 21, 2018)

Models of porous media are often applied to relatively small systems, which leads not only to system-size-dependent results, but also to phenomena that would be absent in larger systems. Here we investigate one such finite-size effect: anisotropy of the permeability tensor. We show that a non-zero angle between the external body force and macroscopic flux vector exists in three-dimensional periodic models of sizes commonly used in computer simulations and propose a criterion, based on the system size to the grain size ratio, for this phenomenon to be relevant or negligible. The finite-size anisotropy of the porous matrix induces a pressure gradient perpendicular to the axis of a porous duct and we analyze how this effect scales with the system and grain sizes.

PACS numbers: 47.56.+r, 47.15.G-, 91.60.Np

## I. INTRODUCTION

For technical reasons pore-scale simulations of flow through porous media are based on simplified, finite-size models. For example, it is not unusual for a numerical model of a bed of sand to contain only 8 “sand grains” [1], and typical values of the ratio of the system size to the grain diameter,  $L/a$ , used in numerical simulations of three-dimensional (3D) flows range from  $\approx 31$  [2] through 17 [3, 4], 10 [5], 8 [6, 7], 3 [8] down to only 2 [1]. Numerical systems with a small value of  $L/a$  are likely to be smaller than the representative elementary volume (REV) of the porous medium they model [9]. Consequently, results of many numerical simulations can contain some systematic errors if this fact has not been properly accounted for.

The basic macroscopic law for creeping flow through a porous medium is Darcy’s law,

$$\mathbf{q} = -\hat{\mathbf{K}}(\nabla P - \rho \mathbf{g}) \quad (1)$$

where  $\mathbf{q}$  is the volumetric fluid flux,  $\hat{\mathbf{K}}$  is a symmetric tensor of the hydraulic conductivity,  $\rho$  is the fluid density,  $\mathbf{g}$  is an external bulk force per unit mass, e.g., gravity, and  $\nabla P$  is the pressure gradient [10]. If the system under consideration is smaller than the REV,  $\hat{\mathbf{K}}$  becomes dependent on a particular realisation of the porous medium, and its components can be regarded as random variables. In particular, a small-size sample of an isotropic medium can exhibit quite high anisotropy. Analysis of the anisotropy of  $\hat{\mathbf{K}}$  as a function of the system size can thus serve as a way to estimate the size of the REV in computer simulations or in some small-scale experiments, e.g., particle image velocimetry [11].

The finite-size anisotropy of a statistically uniform porous medium can be estimated by the dispersion  $\sigma_\alpha$  of the angle  $\alpha$  between the volumetric fluid flux ( $\mathbf{q}$ ) and the driving force ( $\rho \mathbf{g} - \nabla P$ ) about its mean value. Using some phenomenological arguments, we proposed [12] a

general relation

$$\sigma_\alpha \propto L^{-\delta}, \quad \delta = d/2, \quad (2)$$

where  $d$  denotes the space dimension and  $L$  is the system size, and verified it numerically for two-dimensional (2D) and quasi one-dimensional models. The aim of the present study is to investigate finite-size anisotropy of statistically uniform porous media in the more realistic three-dimensional case.

## II. MODEL

As visualised in Fig. 1, we model the porous matrix as a system of identical, impenetrable cubes of side  $a$  randomly distributed in a cuboidal duct. The cubes are aligned along the edges of the system, they are free to overlap and their number depends on the target porosity. The system is always periodic along the duct axis and in the remaining two directions either periodic boundary conditions or no-slip, impenetrable walls are assumed. Due to periodicity, the pressure gradient along the duct axis vanishes. The fluid is set in motion by a body force directed along the duct axis. The fluid is also assumed to be incompressible and its velocity is small enough to ensure that the flow is in the Darcy regime. Models of this type were studied, for example, in Refs. [13–16] and more recently in [17].

## III. SIMULATION METHODS

We chose the lattice Boltzmann method (LBM) as the main simulation method. In this approach, the simulation domain is discretized into a regular lattice and the fluid is described by a mesoscopic particle distribution function defined on all nodes of the lattice. The mesoscopic velocity is also discretized, allowing momentum

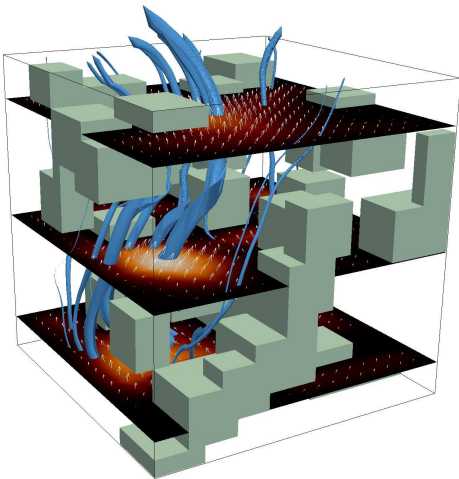


FIG. 1. (Color online) Exemplary realisation of a porous matrix and the corresponding flow solution. The matrix is composed of overlapping solid cubes and periodic boundary conditions are assumed in all directions. Small arrows show the velocity field and its magnitude is represented by the thickness of streamtubes and the brightness of the color on the horizontal cross-sections. The porosity  $\varphi = 0.7$ .

and mass transfer between selected neighboring nodes only. In this work, we use the D3Q19 lattice with the so-called multi-relaxation times (MRT) collision operator [18]. For non-slip boundary conditions, we use the bounce-back rule and body forces are implemented using Guo’s method [19]. This method can be shown to reproduce the Navier-Stokes equations with second-order accuracy. We refer the reader to Refs. [20, 21] for a more detailed discussion of the LBM.

Of many implementations of the LBM we chose the Sailfish library (<http://sailfish.us.edu.pl>). A unique feature of Sailfish is that it runs on graphics processing units (GPUs), which allows for significant speedups as compared to typical CPU codes [22]. Sailfish automatically generates optimized GPU code based on a high-level model description consisting in a large part of formulas in a computer algebra system (SymPy). The code takes advantage of the intrinsic parallelism of the lattice Boltzmann method by assigning individual lattice nodes to separate threads on the GPU. These threads then execute almost independently, only exchanging data with nearest neighbors in the streaming step of the LB algorithm. The details of the implementation and code optimization techniques exploited in the library will be presented elsewhere.

One of the main drawbacks of the LBM is that it is based on a regular lattice. This means that a porous matrix is actually approximated by a set of small cubes (mesh cells) and may contain many artificial edges and vertices. This, in turn, introduces relatively large errors into the flow solution at nearby mesh cells. A solution obtained on a regular lattice can be thus regarded either as an approximate solution for given boundary conditions

or as a valid solution for a model where only an approximate location of the boundaries is known. While in principle this uncertainty could be reduced by increasing the mesh resolution, this approach could quickly exhaust all available computer resources.

Instead, we verified the LBM solutions by the finite volume method (FVM). In this approach the space is divided into a mesh of polyhedrons which are then used, through volume integrals, to express the Navier-Stokes equations in the form of algebraic equations. Meshing was performed with the snappyHexMesh (SHM) utility from the OpenFOAM toolkit [23]. Due to hardware limitations, the number of cells was limited to  $\approx 2$  million. The flow equations were solved with OpenFOAM’s icoFoam solver, which is an open-source implementation of the PISO algorithm [24], a well-established method of computational fluid dynamics. The code of icoFoam was modified to adjust it to the needs of our simulations, e.g. handling of the external force  $\mathbf{g}$ . While PISO allows for much larger time steps than the LBM and can be run on unstructured meshes adjusted to the local geometry of the porous medium, it turned out far more time- and resource-consuming, therefore we used it only for verification purposes on relatively small systems.

By varying the magnitude of driving force we checked that the flow is well within the Darcy regime. To ensure that the steady-state had actually been reached, for systems with periodic boundary conditions we monitored the temporal evolution of the angle  $\alpha$  between the external body force  $\mathbf{g}$  and the resulting Darcy flux  $\mathbf{q}$  and continued the simulations until

$$|\alpha(k) - \alpha(k - N)| \leq \varepsilon |\alpha(k - N)|, \quad (3)$$

where  $k$  is the LBM or PISO iteration number,  $\varepsilon = 10^{-6}$ , and  $N = 2 \times 10^4$  or  $N = 500$  for the LBM and PISO, respectively. In the case of a solid wall channel we used an alternative stopping criterion,

$$\sqrt{\frac{\sum_i |\mathbf{u}_i(k) - \mathbf{u}_i(k - N)|^2}{\sum_i |\mathbf{u}_i(k)|^2}} \leq \varepsilon. \quad (4)$$

where  $\mathbf{u}_i$  is the local velocity at cell  $i$ .

To verify our computational procedures, we applied both the LBM and PISO to determine the permeability of a simple cubic arrangement of overlapping spheres. This standard problem was already investigated with several independent numerical methods and reference solutions are available for comparison [25, 26]. We found the permeabilities computed with both methods to be in acceptable agreement (a few percent) with the reference values (data not shown).

## IV. RESULTS

### A. Periodic boundary conditions

If the system has periodic boundary conditions in all directions, the angle  $\alpha$  between the body force  $\mathbf{g}$  and the

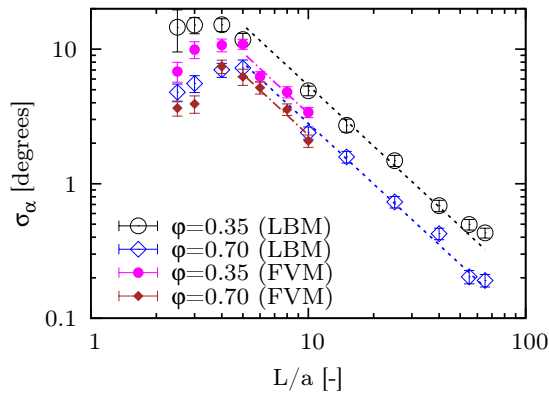


FIG. 2. (Color online) Dispersion of the angle between the flow direction ( $\mathbf{q}$ ) and the external force ( $\mathbf{g}$ ) as a function of the system size  $L$  for two porosities  $\varphi$  and  $a = 4$  l.u. Open and filled symbols correspond to the LBM and FVM (PISO) solvers, respectively. Dashed lines are the best fits to the theoretical formula  $\sigma_\alpha \propto (L/a)^{-3/2}$  for  $L/a \geq 5$ . Error bars represent the standard errors of the mean calculated from 25 independent samples.

Darcy flux  $\mathbf{q}$  is usually nonzero and its standard deviation,  $\sigma_\alpha$ , taken over an ensemble of porous samples, is expected to depend on the system size  $L$  in accordance with Eq. (2). To verify whether this equation holds for 3D systems, we generated hundreds of independent porous samples, as described in Sec. II, with  $a = 4$  lattice units (l.u.). We chose two target porosities,  $\varphi = 0.35, 0.7$ , lying between the porosity below which the flow is completely blocked,  $\varphi_b \approx 0.1$ , and the percolation threshold (for overlapping cubes) above which the porous matrix splits into disjoint clusters,  $\varphi_p \approx 0.77$ . Simulations were performed for several system sizes  $L$  ranging from 10 to 260 l.u. and the results were averaged over 25 independent samples. The number of obstacles per sample varied from  $\approx 6$  ( $L/a = 2.5$ ,  $\varphi \approx 0.7$ ) to  $\approx 284\,000$  ( $L/a = 65$ ,  $\varphi \approx 0.35$ ). The actual porosity of a random sample could differ from the target porosity by  $\approx 5\%$  for  $L/a = 2.5$  and by  $\approx 0.03\%$  for  $L/a = 65$ .

The results, shown in Fig. 2, are in good agreement with Eq. (2). It is interesting to notice that this asymptotic formula describes the system behavior even for as small values of  $L/a$  as 5. As expected [12], the finite-size anisotropy increases as the porosity is decreased, which can be related to the fact that the flow in low-porosity media is more tortuous, a factor particularly important close to the percolation threshold.

Comparison of the results obtained with the PISO and the LBM reveals that the former tends to give systematically smaller values of  $\sigma_\alpha$ . Nevertheless, both methods yield the same value of  $\delta \approx 3/2$  in Eq. (2). We checked that the discrepancy between the results could be significantly reduced by using finer meshes, at the cost of one being forced to consider smaller system sizes due to hardware limits (data not shown). Because of complex

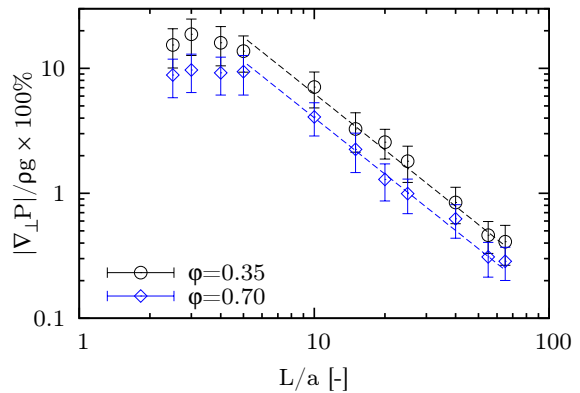


FIG. 3. (Color online) LBM results for the magnitude of the induced pressure gradient,  $|\nabla_\perp P|$ , normalized by the hydrostatic pressure gradient,  $\rho g$ , averaged over 25 configurations. The dashed lines are the best fits to  $|\nabla_\perp P|/\rho g \propto (L/a)^{-3/2}$  for  $L/a \geq 5$ .

meshing, PISO turned out to be particularly costly in terms of computer time and resources. For example, a single PISO simulation for the case of  $L/a = 10$  took  $\approx 7$  hours (including the meshing) and required 4 GB of RAM on a single core of an AMD Opteron 2384 processor, whereas the Sailfish code running on a Tesla M2090 GPU would solve the same case in less than 5 minutes, requiring only about 12 MB of storage. For this reason we did not use PISO for systems with  $L/a > 10$ . Detailed comparison of the two methods in the context of porous media studies will be discussed elsewhere.

## B. No-slip boundary conditions

If a porous medium is placed inside a long, straight channel with impermeable walls then the mean fluid velocity will be parallel to the channel boundaries irrespective of the direction of the driving force  $\mathbf{g}$ . If the medium is anisotropic then a pressure gradient  $\nabla_\perp P$  perpendicular to the channel axis must develop for Darcy's law, Eq. (1), to be satisfied.

To investigate this effect we used the same model as in Sec. IV A except for the no-slip boundary conditions imposed on the channel walls. The results, obtained with the LBM for several values of  $\varphi$  and  $L/a$  and normalized by the gradient of the hydrostatic pressure acting along the channel, are depicted in Fig. 3. As expected, the dependence of  $|\nabla_\perp P|$  on the system size turns out similar to that of  $\sigma_\alpha$  in periodic systems, i.e.,  $|\nabla_\perp P| \propto L^{-3/2}$  for  $L/a \gtrsim 5$ . This result can be generalized to systems of arbitrary space dimension  $d$  and expressed in a dimensionless form as follows,

$$\frac{|\nabla_\perp P|}{\rho g} \propto \left(\frac{L}{a}\right)^{-d/2}, \quad \text{for } L/a \gg 1. \quad (5)$$

### C. Condition for the induced pressure gradient to vanish

Equation (1) implies that it is possible to eliminate the induced pressure gradient by replacing  $\mathbf{g}$  with

$$\mathbf{g}' = \mathbf{g} + \nabla_{\perp} P(\mathbf{g})/\rho \quad (6)$$

where  $\nabla_{\perp} P(\mathbf{g})$  denotes the pressure gradient induced by  $\mathbf{g}$ . Let  $\beta$  denote the angle between  $\mathbf{g}'$  and the channel axis. Equation (5) can be now rewritten as

$$\tan \beta \propto \left(\frac{L}{a}\right)^{-\delta}. \quad (7)$$

As  $\beta$  is small, this formula can be further simplified to

$$\beta \propto \left(\frac{L}{a}\right)^{-\delta}. \quad (8)$$

This means that  $\beta$  decreases with an increasing system size in the same way as  $\sigma_{\alpha}$  does, cf. Eq. (2).

### D. The size of the REV

Generally, the size of the REV depends on many factors, including the required accuracy of measurements. Its magnitude can be estimated in our model based on the dependence of  $\alpha$  or  $|\nabla_{\perp} P|/\rho g$  on the system size. If we make an *ad hoc* assumption that the anisotropy effects are small enough to be practically negligible for  $\sigma_{\alpha} \lesssim 2^{\circ}$  then from Fig. 2 one can estimate the size of the REV to be  $\approx 20a$ . This value agrees with the data in Fig. 3, which shows that for  $L/a > 20$  the induced pressure gradient is smaller than 2% of the pressure gradient driving the fluid through the duct. This enables to estimate the size of the REV in the model considered here as  $\approx 80 \times 80 \times 80$  l.u. Note that since the finite-size anisotropy effects grow as the porosity is lowered, cf. Figs. 2 and 3, the size of the REV is also expected to increase as  $\varphi$  is decreased. For porosities close to  $\varphi_b$ , which is the percolation threshold for the pore space, the size of the REV is expected to grow to infinity.

## V. DISCUSSION OF THE RESULTS AND CONCLUSIONS

Pore-scale computer simulations of transport through porous media are very resource-intensive and hence are often performed on systems whose size is smaller than the representative elementary volume, which makes the

results system-size-dependent. In particular, statistically generated homogeneous porous media smaller than the REV can exhibit significant anisotropy. We have confirmed the hypothesis that various measures of this finite-size anisotropy decrease with the system size  $L$  as  $L^{-\delta}$  with  $\delta = -3/2$ . These measures include the angle between the driving force and the resulting volumetric fluid flux in systems with periodic boundary conditions as well as the pressure gradient induced in flows through solid wall channels. By taking  $\delta = -d/2$ , this conclusion can be generalized to quasi one-dimensional ( $d = 1$ ) and quasi two-dimensional ( $d = 2$ ) flows [12].

Perhaps the most important observation is that the  $L^{-\delta}$  scaling holds for systems much smaller than the REV. This implies that computer simulations of macroscopic systems can be performed using relatively small, “mesoscopic” models, provided that the results will be extrapolated to macroscopic scales using appropriate scaling. Moreover, since the  $L^{-\delta}$  scaling can be theoretically related to the central limit theorem [12], a porous medium can be regarded as consisting of essentially *independent* volumes *much smaller* than the REV. This should facilitate not only numerical, but also theoretical investigation of transport in porous media.

Our results were obtained for a particular choice of a porous medium which was modelled as a union of overlapping objects of the same size and shape. We expect that our conclusions are quite general and are also valid for other classes of statistically uniform porous media, e.g. for polydisperse porous media or for porous matrices generated using different algorithms, e.g. by convoluting random fields with Gaussian kernels [27] or by using the data from the X-ray computed tomography [1, 9]. However, this hypothesis needs to be verified independently.

Finally, our work confirms usability of the Sailfish library for investigation of flows in porous media. While the results obtained with this software differ by several percent from the ones obtained using a more traditional approach that is routinely used in computational fluid dynamics (FVM and PISO), both methods yield qualitatively the same results. However, Sailfish, which is an open-source GPU implementation of the lattice Boltzmann method, turns out faster, requires far less computer resources, and can handle much larger problems.

## VI. ACKNOWLEDGMENTS

This work is supported by MNiSW grant No. N 519 437939 (ZK and MM). MJ acknowledges a scholarship from the TWING project cofinanced by the European Social Fund. This research was supported in part by PL-Grid Infrastructure.

---

[1] T. Sugita, T. Sato, S. Hirabayashi, J. Nagao, Y. Jin, F. Kiyono, T. Ebinuma, H. Narita, A Pore-Scale Numerical

ical Simulation Method for Estimating the Permeabil-



- ity of Sand Sediment, *Transport in Porous Media* 94 (1) (2012) 1–17, doi:“bibinfodoi10.1007/s11242-012-9975-2.”
- [2] C. Pan, M. Hilpert, C. T. Miller, Pore-scale modeling of saturated permeabilities in random sphere packings, *Phys. Rev. E* 64 (6) (2001) 066702–+, doi:“bibinfodoi10.1103/PhysRevE.64.066702.”
- [3] M. A. Knackstedt, X. Zhang, Direct evaluation of length scales and structural parameters associated with flow in porous media, *Phys. Rev. E* 50 (1994) 2134–2138, doi:“bibinfodoi10.1103/PhysRevE.50.2134.”
- [4] X. Zhang, M. A. Knackstedt, Direct simulation of electrical and hydraulic tortuosity in porous solids, *Geophys. Res. Lett.* 22 (17) (1995) 2333–2336.
- [5] A. G. Yiotis, J. Psihogios, M. E. Kainourgiakis, A. Papaioannou, A. K. Stubos, A lattice Boltzmann study of viscous coupling effects in immiscible two-phase flow in porous media, *Colloid Surf. A-Physicochem. Eng. Asp.* 300 (2007) 35–49.
- [6] S. Succi, E. Foti, F. Higuera, Three-Dimensional Flows in Complex Geometries with the Lattice Boltzmann Method, *Europhys. Lett.* 10 (5) (1989) 433–438.
- [7] A. Cancelliere, C. Chang, E. Foti, D. Rothman, S. Succi, The permeability of random medium: Comparison of simulation with theory, *Phys. Fluids A* 2 (12) (1990) 2085–2088.
- [8] R. Verberg, A. J. C. Ladd, Simulation of low-Reynolds-number flow via a time-independent lattice-Boltzmann method, *Phys. Rev. E* 60 (1999) 3366–3373.
- [9] D. Zhang, R. Zhang, S. Chen, W. E. Soll, Pore scale study of flow in porous media: Scale dependency, REV, and statistical REV, *Geophysical Research Letters* 27 (8) (2000) 1195–1198, ISSN 1944-8007.
- [10] J. Bear, *Dynamics of Fluids in Porous Media*, Elsevier, New York, 1972.
- [11] M. Morad, A. Khalili, Transition layer thickness in a fluid-porous medium of multi-sized spherical beads, *Experiments in Fluids* 46 (2009) 323–330.
- [12] Z. Koza, M. Matyka, A. Khalili, Finite-size anisotropy in statistically uniform porous media, *Phys. Rev. E* 79 (6) (2009) 066306, doi:“bibinfodoi10.1103/PhysRevE.79.066306.”
- [13] A. F. Morais, H. Seybold, H. J. Herrmann, J. S. Andrade, Non-Newtonian Fluid Flow through Three-Dimensional Disordered Porous Media, *Phys. Rev. Lett.* 103 (2009) 194502, doi:“bibinfodoi10.1103/PhysRevLett.103.194502,” URL <http://link.aps.org/doi/10.1103/PhysRevLett.103.194502>.
- [14] M. M. Tomadakis, S. V. Sotirchos, Transport properties of random arrays of freely overlapping cylinders with various orientation distributions, *J. Chem. Phys.* 98 (1993) 616–626.
- [15] A. Koponen, M. Kataja, J. Timonen, Permeability and effective porosity of porous media, *Phys. Rev. E* 56 (1997) 3319–3325, doi:“bibinfodoi10.1103/PhysRevE.56.3319,” URL <http://link.aps.org/doi/10.1103/PhysRevE.56.3319>.
- [16] M. Matyka, A. Khalili, Z. Koza, Tortuosity-porosity relation in porous media flow, *Phys. Rev. E* 78 (2008) 026306, doi:“bibinfodoi10.1103/PhysRevE.78.026306,” URL <http://link.aps.org/doi/10.1103/PhysRevE.78.026306>.
- [17] A. Duda, Z. Koza, M. Matyka, Hydraulic tortuosity in arbitrary porous media flow, *Phys. Rev. E* 84 (2011) 036319, doi:“bibinfodoi10.1103/PhysRevE.84.036319,” URL <http://link.aps.org/doi/10.1103/PhysRevE.84.036319>.
- [18] D. d’Humières, I. Ginzburg, M. Krafczyk, P. Lallemand, L.-S. Luo, Multiple-relaxation-time lattice Boltzmann models in three dimensions, *Phil. Trans. R. Soc. Lond. A* 360 (2002) 437–451.
- [19] Z. Guo, C. Zheng, B. Shi, Discrete lattice effects on the forcing term in the lattice Boltzmann method, *Phys. Rev. E* 65 (4) (2002) 046308–+, doi:“bibinfodoi10.1103/PhysRevE.65.046308.”
- [20] S. Chen, G. D. Doolen, Lattice Boltzmann Method for Fluid Flows, *Annual Review of Fluid Mechanics* 30 (1) (1998) 329–364, doi:“bibinfodoi10.1146/annurev.fluid.30.1.329.”
- [21] C. K. Aidun, J. R. Clausen, Lattice-Boltzmann Method for Complex Flows, *Annual Review of Fluid Mechanics* 42 (1) (2010) 439–472, doi:“bibinfodoi10.1146/annurev-fluid-121108-145519.”
- [22] J. Tölke, M. Krafczyk, TeraFLOP computing on a desktop PC with GPUs for 3D CFD, *Int. J. Comput. Fluid Dyn.* 22 (7) (2008) 443–456.
- [23] H. G. Weller, G. Tabor, H. Jasak, C. Fureby, A tensorial approach to computational continuum mechanics using object-oriented techniques, *Computers in Physics* 12 (6) (1998) 620–631, doi:“bibinfodoi10.1063/1.168744,” URL <http://link.aip.org/link/?CIP/12/620/1>.
- [24] J. H. Ferziger, M. Perić, *Computational Methods for Fluid Dynamics*, Springer, 3rd edn., 2002.
- [25] R. E. Larson, J. J. L. Higdon, A periodic grain consolidation model of porous media, *Phys. Fluids A* 1 (1989) 38–46.
- [26] D. W. Holmes, J. R. Williams, P. Tilke, Smooth particle hydrodynamics simulations of low Reynolds number flows through porous media, *International Journal for Numerical and Analytical Methods in Geomechanics* 35 (4) (2011) 419–437, ISSN 1096-9853.
- [27] J. D. Hyman, P. K. Smolarkiewicz, C. L. Winter, Heterogeneities of flow in stochastically generated porous media, *Phys. Rev. E* 86 (2012) 056701, doi:“bibinfodoi10.1103/PhysRevE.86.056701,” URL <http://link.aps.org/doi/10.1103/PhysRevE.86.056701>.